NANO LETTERS

Letter

pubs.acs.org/NanoLett

The Bright Future for Electrode Materials of Energy Devices: Highly Conductive Porous Na-Embedded Carbon

Wei Wei,[†] Liang Chang,[†] Kai Sun,[‡] Alexander J. Pak,[§] Eunsu Paek,[§] Gyeong S. Hwang,[§] and Yun Hang Hu*[,†]

[†]Department of Materials Science and Engineering, Michigan Technological University, 1400 Townsend Drive, Houghton, Michigan 49931-1295, United States

[‡]Department of Materials Science and Engineering, University of Michigan, Ann Arbor, Michigan 48109-2136, United States

[§]Department of Chemical Engineering, University of Texas at Austin, Austin, Texas 78712-1589, United States

Supporting Information

ABSTRACT: High electrical conductivity and large accessible surface area, which are required for ideal electrode materials of energy conversion and storage devices, are opposed to each other in current materials. It is a long-term goal to solve this issue. Herein, we report highly conductive porous Na-embedded carbon (Na@C) nanowalls with large surface areas, which have been synthesized by an invented reaction of CO with liquid Na. Their electrical conductivities are 2 orders of magnitude larger than highly conductive 3D graphene. Furthermore, almost all their surface areas are accessible for electrolyte ions. These unique properties make them ideal electrode materials for energy devices, which significantly surpass expensive Pt. Consequently, the dye-sensitized solar cells (DSSCs) with the Na@C counter electrode has reached a high power conversion efficiency of 11.03%. The Na@C also exhibited excellent performance for supercapacitors, leading to high capacitance of 145 F g^{-1} at current density of 1 A g^{-1}.

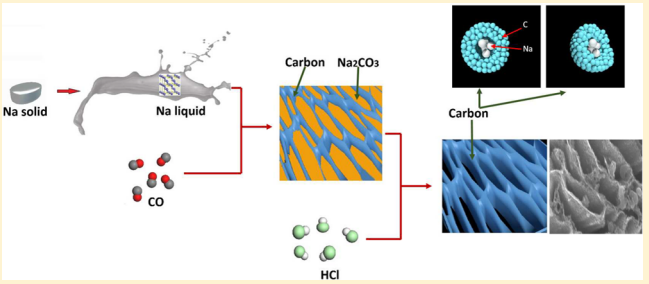

KEYWORDS: *Na-embedded carbon, electrode materials, DSSCs, supercapacitor*

Carbon, which has many allotropes, is one of the most important materials for electrical devices, such as rechargeable batteries, capacitors, fuel cells, and solar cells. Ideal electrode materials must possess both high electrical conductivity and large accessible surface area. Graphite has high conductivity but very low surface area. In contrast, amorphous carbon has a large surface area but low conductivity. Among all of these carbon materials, pristine graphene has the highest conductivity with large surface area.[1] However, without a substrate, graphene sheets can readhere into graphite to lose surface area or crumple three-dimensionally with damaging conductivity. Therefore, it is a challenging task to solve the contradiction between high electrical conductivity and large surface area for electrode materials.

Doping alkali metals into carbon materials has been demonstrated to create highly conductive carbon materials.[2−6] However, as the dopants are located on the carbon surface, they can be easily oxidized, leading to a decrease in conductivity. To solve this issue, alkali metal atoms must be completely surrounded by carbon atoms to form alkali-metal-embedded carbon material. Such a hypothetical material is totally different from widely used intercalation carbon compounds in which alkali ions are inserted into spaces between graphite layers.[7,8] So far, however, the alkali-metal-embedded carbon material has not yet been successfully synthesized.

In this work, we successfully synthesized highly conductive porous Na-embedded carbon nanowall materials (with large accessible surface areas) using an original reaction between liquid Na and CO gas. The novel materials solve the critical issue "the contradiction between high electrical conductivity and large accessible surface area" in current electrode materials. Furthermore, the fabricated materials were tested as electrodes for energy devices, leading to high power conversion efficiency of 11.03% for a dye-sensitized solar cell (DSSC) and large capacitance of 145 F g^{-1} for a supercapacitor.

It is unlikely to synthesize alkali-metal-embedded carbon using current doping techniques, with which dopants are introduced into the presynthesized carbon so that dopants are located on its surface but not inside it. In this work, we propose a novel strategy in which alkali-metal atoms are embedded inside carbon during carbon formation. First, we design the following reaction between CO and liquid Na:

$$Na_{(1)} + 3/2CO_{(g)} \rightarrow C + 1/2Na_2CO_{3(s)} \quad (1)$$

This reaction is supported by our thermodynamic calculations (Figure S1). The negative changes of Gibbs free energy and enthalpy of this reaction confirm its thermodynamic

Received: November 12, 2016
Published: November 22, 2016

DOI: 10.1021/acs.nanolett.6b04742
Nano Lett. 2016, 16, 8029−8033

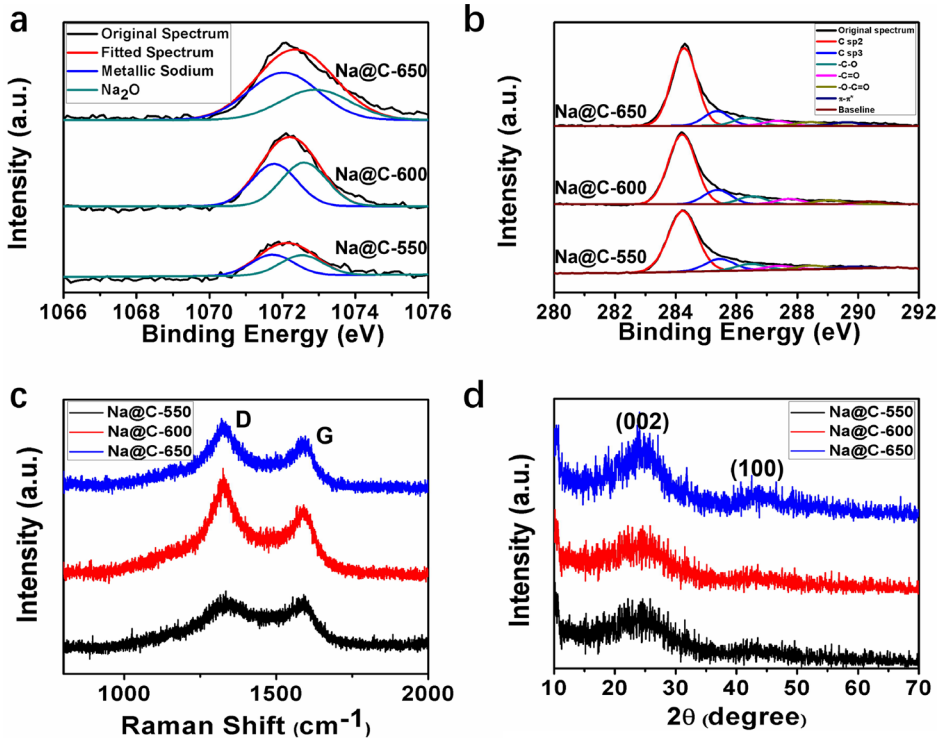

Figure 1. Structure and composition evaluation of Na-embedded carbon materials synthesized from reaction between Na and CO (followed by HCl acid treatment and water washing). (a) XPS spectra of Na 1s. (b) XPS spectra of C 1s. (c) Raman spectra. (d) XRD patterns. (Na-embedded carbon materials synthesized at 550, 600, and 650 °C are denoted as Na@C-550, Na@C-600, and Na@C-650, respectively.)

spontaneity and energy efficiency, respectively. During the carbon formation, some Na atoms are predicted to be embedded inside the carbon material (hereafter referred to as Na@C), and the reaction (eq 1) can be rewritten as follows:

$$x\mathrm{Na}_{(1)} + y\mathrm{CO}_{(g)} \rightarrow \mathrm{Na@C}_n + z\mathrm{Na}_2\mathrm{CO}_{3(s)} \quad (2)$$

Furthermore, the simultaneously formed Na_2CO_3 can control the shape of Na@C. After Na_2CO_3 nanoparticles are removed by acid, mesopores are formed to produce porous Na@C. This strategy is validated by the following experiments.

For Na@C synthesis, 50 mmol of Na metal was placed in a ceramic tube reactor and followed by the introduction of CO gas at 50 psi and room temperature. The temperature increased to a selected temperature (550, 600, or 650 °C) by 10 °C min^{-1} and then held for 48 h. The obtained products were subjected to X-ray diffraction (XRD) measurements. As shown in Figure S2, diffraction peaks indicative of Na_2CO_3 confirm the reaction between Na and CO. Hydrochloric acid was then used to remove Na_2CO_3, followed by washing with deionized water. The obtained black powder was identified as carbon by elemental analysis (Table S1). Furthermore, inductively coupled plasma (ICP) and X-ray photoelectron spectroscopy (XPS) were exploited to identify the existence of metallic Na inside the carbon. As shown in Table S1, ICP analysis shows that there are 2.1, 2.7, and 1.8 wt % Na in the C materials synthesized at 550, 600, and 650 °C, respectively. In the energy region of Na 1s, one can see a broad peak centered at 1072 eV in XPS spectrum (Figure 1a). Deconvolution of this peak reveals two peaks associated with metallic Na (1071.7 eV) and Na^+ ions (1072.5 eV).[9,10] The existence of metallic Na indicates that some metallic Na atoms were successfully embedded inside carbon as they were not oxidized when treated by hydrochloric acid and washed with water. The ratio of metallic Na atoms to Na^+ ions is nearly 1:1 for all three samples; the combination of XPS and ICP reveals that 1.1, 1.3, and 1.0 wt % metallic Na atoms were embedded inside C synthesized at 550, 600, and 650 °C, respectively, which are denoted as Na@C-550, Na@C-600, and Na@C-650.

Furthermore, XPS was also used to evaluate the content of the sp^2 and sp^3 bonded carbon as well as oxygen groups. As shown in Figure 1b, the deconvolution of the C 1s peak revealed five components centered at 284.8, 285.5, 286.7, 287.8, and 288.9 eV, which are associated with sp^2 carbon atoms, sp^3 carbon atoms, −C-O, −C═O, and −O−C═O groups, respectively.[11,12] The main component is sp^2 bonded carbon (69.8−79.6%), whereas sp^3 carbon (13.9−15.0%) and oxygen groups (5.3−16.2%) constitute a small fraction of the materials (Table S2). The sp^2 carbon increases with increasing synthesis temperature. The carbon structure of Na@C was further evaluated by Raman. It is well-demonstrated that the Raman D band at about 1355 cm^{-1} can be assigned to the breathing mode of aromatic rings with dangling bonds (disordered graphene π systems) and the G band at about 1575 cm^{-1} attributed to the bond stretching of sp^2 carbon pairs.[13] Figure 1c shows both D and G bands, indicating the existence of aromatic rings with dangling bonds (associated with defected and functionalized carbon) and sp^2 bonded carbon. This is consistent with XPS results.

The XRD pattern shows a broad diffraction peak at 2θ = 24.7° (Figure 1d), indicating that the Na@C materials are amorphous. Furthermore, field emission scanning electron microscopy (FESEM) shows that the material possesses porous structure with nanowalls of about 50 nm thickness (Figure 2a), which was supported by transmission electron microscopy (TEM) images (Figure 2b). The electron diffraction pattern in

DOI: 10.1021/acs.nanolett.6b04742
Nano Lett. 2016, 16, 8029−8033

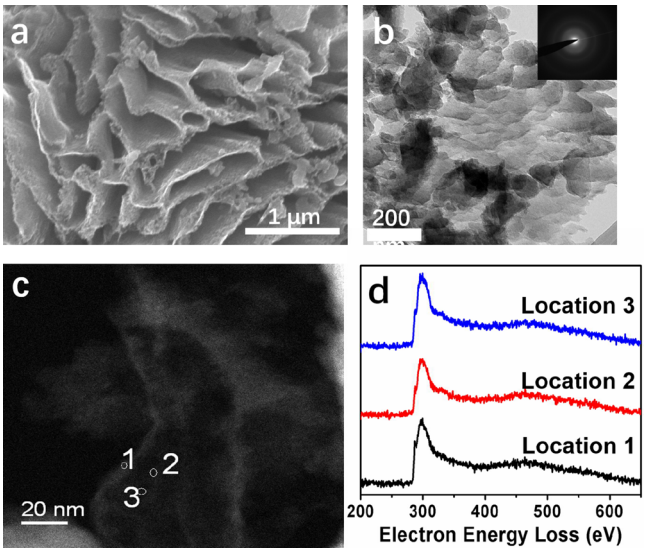

Figure 2. Characterization of Na@C-600. (a) FESEM image. (b) TEM image with electron diffraction pattern inset. (c) High-angle annular dark field (HAADF) image. (d) EELS at locations 1−3 in (c).

TEM further confirms the amorphous structure (Figure 2b). Electron energy loss spectra (EELS) exhibit an intensive feature of sp^2-bonded carbon atoms in the carbon K-edge region (Figure 2c,d): a peak at 285 eV due to transitions from the 1s to the π^* state ($1s-\pi^*$) and a peak at 291 eV corresponding to transitions from the 1s to the σ^* state ($1s-\sigma^*$).[14,15]

Surface areas and pore size distributions were determined by N_2 adsorption at liquid nitrogen temperature. The BET surface areas are 625, 345, and 301 $m^2\ g^{-1}$ for Na@C-550, Na@C-600, and Na@C-650, respectively (Table S3), which indicates that the surface area decreases with increasing synthesis temperature. In addition, the materials possess mesopores and macropores (Figure S3), which enable liquid diffusion through the pores. This was supported by their accessible surface areas. From the adsorbed charges associated with electrolyte (Figure S4), we calculated electrolyte-accessible surface areas of 600, 329, and 262 $m^2\ g^{-1}$ for Na@C-550, Na@C-600, and Na@C-650, respectively (Table S3). The accessible surface areas are very close to their corresponding total surface areas, indicating that surfaces of Na@C materials are nearly entirely accessible for electrolyte ions, which is desired for electrode materials.

The electrical conductivities of the Na@C samples were measured by the four-point probe method and ranged between 273−524 S cm^{-1} (namely, 273 S cm^{-1} for Na@C-550, 384 S cm^{-1} for Na@C-600, and 524 S cm^{-1} for Na@C-650). The conductivity tends to increase with high synthesis temperature due to the increase in sp^2 carbon content by annealing. Furthermore, they are 2 orders of magnitude larger than 3D graphene (2−3 S cm^{-1}).[16,17] To theoretically validate the role of the dopants, we solved the Boltzmann transport equation (BTE) using the BoltzTrap program[18] interfaced with VASP.[19] As seen in Figure 3a, a porous carbon structure was generated and subsequently filled with 2 wt % Na. Figure 3b compares the semiclassical ratio of the electrical conductivity and scattering time (σ/τ) to the electron carrier density (n). Assuming the scattering times are comparable in the embedded and unembedded cases, it is evident that the presence of embedded-Na can increase σ 2-fold. We attribute this primarily to the decrease in the effective mass (m^*) of π electrons due to embedded-Na polarization, as evidenced by the broadening of the dispersion near the Fermi level (Figure S6). However, given that previous experiments demonstrate that K impurities suppress the electron mobility ($\mu \propto \tau/m^*$) in graphene,[4] we estimate that the increase in σ is far larger than 2-fold.

The high conductivity and large accessible surface area of Na@C materials make them excellent electrode candidates for energy devices, which are confirmed as follows:

Electricity produced from commercial silicon photovoltaics is still expensive. This has promoted intensive attempts to develop newer alternatives for the Si solar cells. One of them is dye-sensitized solar cells (DSSCs), which have unique advantages, such as simple fabrication procedure and lower cost.[20−25] A typical DSSC, which consists of N719 ruthenium dye, I^-/I_3^- electrolyte, and Pt CE, has a power conversion efficiency (PCE) of about 7−8%. In the past 10 years, the PCEs of DSSCs have increased up to 12% through numerous breakthroughs for dyes and electrolytes.[21−24] However, innovations of CE have not yet been obtained for similarly significant improvements in PCE, even though various

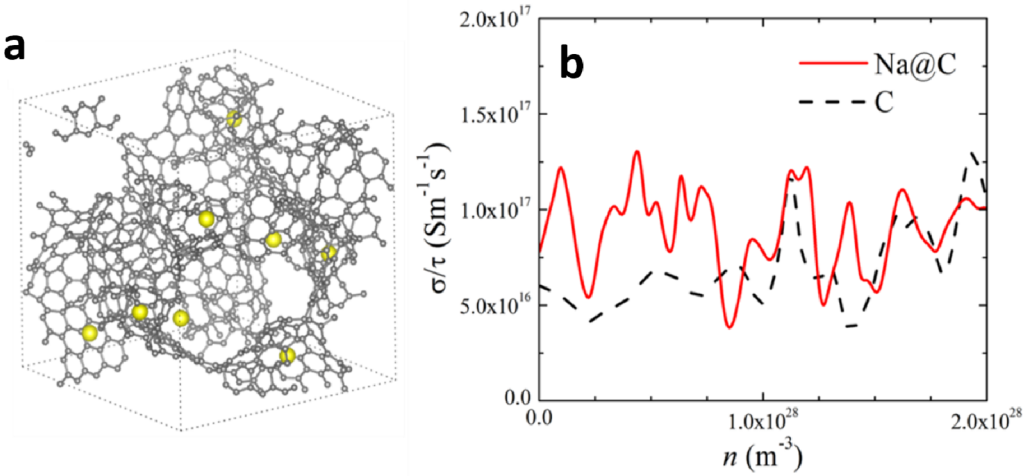

Figure 3. Theoretical evaluation of electrical conductivity. (a) Schematic of the simulated porous carbon structure (gray balls/sticks) with 2 wt % Na (yellow balls). (b) Computed ratio of electrical conductivity to relaxation time (σ/τ) from the solution to the Boltzmann transport equation.

DOI: 10.1021/acs.nanolett.6b04742
Nano Lett. 2016, 16, 8029−8033

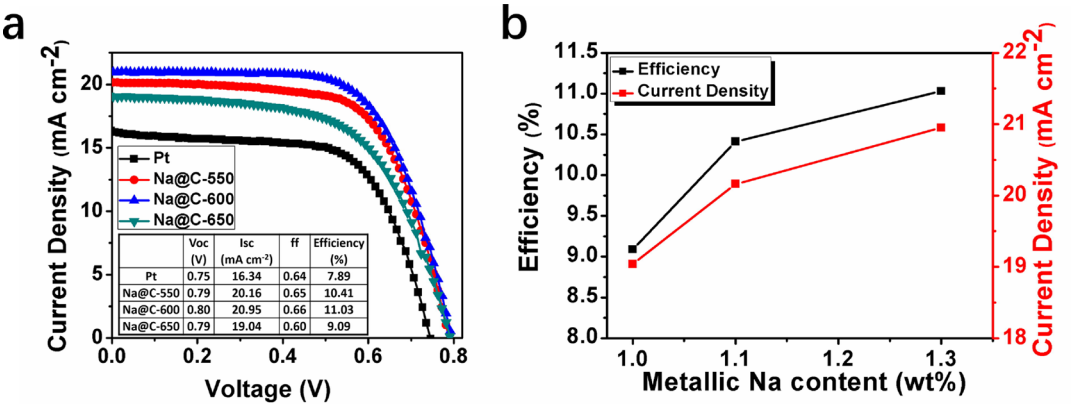

Figure 4. Characterization of DSSCs with Na@C CE. (a) Photocurrent density−voltage curves and performance parameters of DSSCs with Pt, Na@C-550, Na@C-600, or Na@C-650 CEs under simulated 1.5G sunlight illumination. (b) The relationship of current density and efficiency with metallic Na content.

materials were explored as a replacement for expensive Pt-based CE.[26,27] Herein, to change this situation, Na@C was exploited as a counter electrode (CE) for DSSCs. The DSSC devices were fabricated with N719 dye-sensitized TiO_2 film, I^-/I_3^- electrolyte, and Na@C CEs. For comparison, a DSSC with a Pt CE was also prepared. Photovoltaic performances of masked cells were evaluated under simulated 1.5G sunlight (100 mW cm^{-2} intensity with wavelengths ranging from 320 to 1100 nm). Their photovoltaic characteristics, including the short-circuit current density (J_{sc}), open-circuit voltage (V_{oc}), fill factor (ff), and PCE (η), are shown in Figure 4a. The DSSC with a Pt CE exhibited PCE of 7.89%, J_{sc} of 16.34 mA cm^{-2}, V_{oc} of 0.75 V, and ff of 0.64. Those are consistent with reported values.[20] Impressively, the best PCE of the DSSC with Na@C-600 CE reached 11.03% (with J_{sc} of 20.95 mA cm^{-2}, V_{oc} of 0.80 V, and ff of 0.66), which is 1.4 times the efficiency (7.89%) with a Pt CE. Such a large increase in PCE is due to the increase of current density from 16.34 mA cm^{-2} with Pt CE to 20.95 mA cm^{-2} with Na@C-600 CE. The performance of the CE is dependent on both the electrical conductivity (for electron transfer) and the catalytic activity (for I_3^- reduction to I^-). Because the conductivity of Pt is larger than Na@C materials, the large increase in current density is attributed to larger absolute catalytic activity using Na@C than Pt. This was confirmed by the evidence that the accessible surface area of Pt is only 0.0022 m^2 g^{-1} (Figure S5), whereas it is 329 m^2 g^{-1} for Na@C-600.

The performance of DSSCs is dependent on the composition of the Na@C material. The PCEs of DSSCs with Na@C CEs are as follows: Na@C-600 (11.03%) > Na@C-550 (10.41%) > Na@C-650 (9.09%). In contrast, their conductivities are in the sequence Na@C-650 > Na@C-600 > Na@C-550, and their surface areas in the sequence Na@C-550 > Na@C-600 > Na@C-650. This indicates that the performance of Na@C CE is not explicitly proportional to either their conductivities or surface areas. Recall that the catalytic activity of CEs is dependent on the total number of active sites (associated with total accessible surface area) and the activity of each active site. Because the observed performance of the Na@C CE is not proportional to surface area, it stands to reason that the activity of each active site for I_3^- reduction changes with composition. As seen in Figure S7, our DFT calculations confirm that I_3^- has larger adsorption energy (E_{ad}) on graphene in the presence of Na on the opposite side. This favorable interaction is likely electrostatic in nature and therefore tends to diminish with additional graphene layers between I_3^- and Na. Indeed, as shown in Figure 4b, the current density and PCE of DSSCs with Na@C CEs are proportional to the content of embedded metallic Na. The importance of Na in the Na@C electrode was also supported by the fact that the efficiency (11.03%) of the DSSC with Na@C CE is much higher than that (8%) of the DSSC with 3D Na-free graphene CE (Figure S10a). The excellent electrocatalytic activity of the Na@C counter electrode was further supported by cyclic voltammogram (CV) evaluation and electrochemical impedance spectrum (EIS) (Figure S11). In addition, the electrode exhibited excellent stability (Figure S12).

The Na@C materials also exhibited excellent performance for supercapacitors (Figure S13). The electrochemical tests of the symmetrical cell with Na@C electrodes were conducted in 2 M KOH at potential range of 0−1 V. As shown in Figure S13, one can see the ideal rectangular CV curve of the Na@C electrode at scan rate of 100 mV s^{-1} and symmetrically triangle galvanostatic charge/discharge profile at current density of 1 A g^{-1}. This indicates the excellent charge propagation on the electrode material surface. Compared with activated carbon (AC) and 3D graphene, the Na@C exhibited the best capacitor performance with the largest CV areas and longest discharge time. The capacity of Na@C electrode reached 145 F g^{-1} at current density of 1 A g^{-1}, which is much higher than 112 F g^{-1} (3D graphene) and 71 F g^{-1} (AC). Even when the current density increased by 10 times to 10 A g^{-1}, the capacity can still remain 114 F g^{-1}. Furthermore, after 5000 times charge/discharge cycles, the capacity retention can be 96.4%, indicating the excellent stability of the Na@C electrode for capacitors.

In conclusion, it is the first time to synthesize hypothetical Na-embedded carbon materials (Na@C), which are porous nanowalls with large surface areas, by an original reaction of CO with liquid Na. Their electrical conductivities are 2 orders of magnitude larger than highly conductive 3D graphene with comparable surface areas. Embedding Na inside carbon not only significantly enhances the conductivity and catalytic activity of carbon but also prevents Na from oxidation by air and electrolytes. Almost all the surface areas of Na@C materials are accessible for electrolyte ions. Therefore, Na@C materials are ideal electrode materials, which are much better than expensive Pt. The DSSC with a Na@C CE reached a high power conversion efficiency of 11.03%. The Na@C material also exhibited excellent performance for supercapacitors. Furthermore, the novel materials can also be applied for

DOI: 10.1021/acs.nanolett.6b04742
Nano Lett. 2016, 16, 8029−8033

other energy conversion and storage devices, such as batteries, fuel cells, and capacitive deionization cells.

■ ASSOCIATED CONTENT

Supporting Information

The Supporting Information is available free of charge on the ACS Publications website at DOI: 10.1021/acs.nanolett.6b04742.

Experimental section, thermodynamic evaluation, characterization of solid products, composition of Na@C materials, pore size distributions, total surface areas and accessible surface areas of Na@C materials, accessible surface areas of Pt film, theoretical prediction of band structures of C and Na@C materials, DFT calculation for I_3^- adsorption on Na@C, IPCE spectra of DSSCs, histogram of efficiencies, comparison between DSSCs with Na@C and 3D graphene as counter electrode, electrocatalytic evaluation and electrochemical impedance characterization, stability of Na@C counter electrode, explanation of counter-electrode-induced V_{oc}, application of Na@C and 3D graphene for supercapacitors (PDF)

■ AUTHOR INFORMATION

Corresponding Author

*E-mail: yunhangh@mtu.edu.

ORCID

Yun Hang Hu: 0000-0002-5358-8667

Author Contributions

Y.H.H. supervised the project and designed the material synthesis approach. W.W. synthesized materials, fabricated DSSC devices, tested the devices' performances, and conducted material characterizations (XRD, SEM, Raman, elemental analysis, and BET). L.C. measured accessible surface areas, fabricated supercapacitor devices, and tested the devices. K.S. performed HAADF-STEM and XPS characterization. G.S.H., A.J.P., and E.P. conducted the computational work with deep analysis. All authors were involved in analysis and discussion of results. Y.H.H. and W.W. wrote the manuscript with input from all other authors.

Notes

The authors declare no competing financial interest.

■ ACKNOWLEDGMENTS

This work was supported by U.S. National Science Foundation (CBET-0931587). The JEOL JEM 3100R05 double Cs-corrected AEM and the Krato XPS were supported by U.S. National Science Foundation (DMR-0723032) and (DMR-0420785), respectively. The computational work was partially supported by the Robert A. Welch Foundation (F-1535). Y.H.H. also thanks Charles and Carroll McArthur for their great support.

■ REFERENCES

(1) Novoselov, K. S.; Geim, A. K.; Morozov, S. V.; Jiang, D.; Zhang, Y.; Dubonos, S. V.; Grigorieva, I. V.; Firsov, A. A. *Science* **2004**, *306*, 666−669.

(2) Haddon, R. C.; Hebard, A. F.; Rosseinsky, M. J.; Murphy, D. W.; Duclos, S. J.; Lyons, K. B.; Miller, B.; Rosamilia, J. M.; Fleming, R. M.; Kortan, A. R.; Glarum, S. H.; Makhija, A. V.; Muller, A. J.; Eick, R. H.; Zahurak, S. M.; Tycko, R.; Dabbagh, G.; Thiel, F. A. *Nature* **1991**, *350*, 320−322.

(3) Hebard, A. F.; Rosseinsky, M. J.; Haddon, R. C.; Murphy, D. W.; Glarum, S. H.; Palstra, T. T. M.; Ramirez, A. P.; Kortan, A. R. *Nature* **1991**, *350*, 600−601.

(4) Chen, J. H.; Jang, C.; Adam, S.; Fuhrer, M. S.; Williams, E. D.; Ishigami, M. *Nat. Phys.* **2008**, *4*, 377−381.

(5) Ohta, T.; Bostwick, A.; Seyller, T.; Horn, K.; Rotenberg, E. *Science* **2006**, *313*, 951−954.

(6) Gao, G.; Çağin, T.; Goddard, W. A. *Phys. Rev. Lett.* **1998**, *80*, 5556−5559.

(7) Tang, K.; Fu, L.; White, R. J.; Yu, L.; Titirici, M. M.; Antonietti, M.; Maier, J. *Adv. Energy Mater.* **2012**, *2*, 873−877.

(8) Wenzel, S.; Hara, T.; Janek, J.; Adelhelm, P. *Energy Environ. Sci.* **2011**, *4*, 3342−3345.

(9) Lee, Y.; Watanabe, T.; Takata, T.; Kondo, J. N.; Hara, M.; Yoshimura, M.; Domen, K. *Chem. Mater.* **2005**, *17*, 2422−2426.

(10) Lotfabad, E. M.; Kalisvaart, P.; Kohandehghan, A.; Karpuzovc, D.; Mitlin, D. *J. Mater. Chem. A* **2014**, *2*, 19685−19695.

(11) Chiang, T.-C.; Seitz, F. *Ann. Phys.* **2001**, *10*, 61−74.

(12) Yumitori, S. *J. Mater. Sci.* **2000**, *35*, 139−146.

(13) Ferrari, A. C.; Meyer, J. C.; Scardaci, V.; Casiraghi, C.; Lazzeri, M.; Mauri, F.; Piscanec, S.; Jiang, D.; Novoselov, K. S.; Roth, S.; Geim, A. K. *Phys. Rev. Lett.* **2006**, *97*, 187401−187404.

(14) Berger, S. D.; McKenzie, D. R.; Martin, P. J. *Philos. Mag. Lett.* **1988**, *57*, 285−290.

(15) Chu, P. K.; Li, L. *Mater. Chem. Phys.* **2006**, *96*, 253−277.

(16) Wang, H.; Sun, K.; Tao, F.; Stacchiola, D. J.; Hu, Y. H. *Angew. Chem., Int. Ed.* **2013**, *52*, 9210−9214.

(17) Wei, W.; Sun, K.; Hu, Y. H. *J. Mater. Chem. A* **2014**, *2*, 16842−16846.

(18) Madsen, G. K. H.; Singh, D. J. *Comput. Phys. Commun.* **2006**, *175*, 67−71.

(19) Kresse, G.; Furthmüller, J. *Phys. Rev. B: Condens. Matter Mater. Phys.* **1996**, *54*, 11169−11186.

(20) O'Regan, B.; Grätzel, M. *Nature* **1991**, *353*, 737−740.

(21) Mathew, S.; Yella, A.; Gao, P.; Humphry-Baker, R.; Curchod, B. F. E.; Ashari-Astani, N.; Tavernelli, I.; Rothlisberger, U.; Nazeeruddin, M. K.; Grätzel, M. *Nat. Chem.* **2014**, *6*, 242−247.

(22) Yella, A.; Lee, H.-W.; Tsao, H. N.; Yi, C.; Chandiran, A. K.; Nazeeruddin, M.; Diau, E. W.-G.; Yeh, C.-Y.; Zakeeruddin, S. M.; Grätzel, M. *Science* **2011**, *334*, 629−634.

(23) Chiba, Y.; Islam, A.; Watanabe, Y.; Komiya, R.; Koide, N.; Han, L. *Jpn. J. Appl. Phys.* **2006**, *45*, L638−L640.

(24) Kinoshita, T.; Dy, J. T.; Uchida, S.; Kubo, T.; Segawa, H. *Nat. Photonics* **2013**, *7*, 535−539.

(25) Xin, X. K.; He, M.; Han, W.; Jung, J. H.; Lin, Z. Q. *Angew. Chem., Int. Ed.* **2011**, *50*, 11739−11742.

(26) Lee, K. S.; Lee, H. K.; Wang, D. H.; Park, N. G.; Lee, J. Y.; Park, O. O.; Park, J. H. *Chem. Commun.* **2010**, *46*, 4505−4507.

(27) Wang, M.; Anghel, A. M.; Marsan, B.; Ha, N. L. C.; Pootrakulchote, N.; Zakeeruddin, S. M.; Grätzel, M. *J. Am. Chem. Soc.* **2009**, *131*, 15976−15977.

DOI: 10.1021/acs.nanolett.6b04742
Nano Lett. 2016, 16, 8029−8033